Journal of Manufacturing Processes 121 (2024) 92–99

Contents lists available at ScienceDirect

Journal of Manufacturing Processes

journal homepage: www.elsevier.com/locate/manpro

Spatial characteristics of ultra hard coating on directed energy deposition (DED)-printed 316L with a novel ultra-fast boriding☆

Himanshu Balhara [a], Cagatay Yelkarasi [b], Ali Erdemir [b], Satish T.S. Bukkapatnam [a,*]

[a] Wm Michael Barns'64 Department of Industrial and Systems Engineering, Texas A&M University, College Station, TX 77840, United States
[b] J.Mike Walker'66 Department of Mechanical Engineering, Texas A&M University, College Station, TX 77840, United States

ARTICLE INFO

Keywords:
Directed energy deposition
Ultra-fast boriding
Microhardness
Microstructure
Morphology

ABSTRACT

Stainless steel 316L, manufactured through Directed Energy Deposition (DED) printing, presents a favorable option for applications in corrosive environments. However, its intrinsic limitation of moderate hardness renders it less suitable for high-wear scenarios. To address this, surface coatings become pivotal in improving surface hardness. In this study, we employed ultra-fast boriding on DED-printed 316L components. The outcomes revealed the formation of a resilient boride layer, 20 μm thick, comprising hard phases with an impressive hardness of 2200 HV ± 200. This marks a substantial tenfold increase from the substrate's initial hardness. Our investigation extends beyond hardness enhancement, delving into the spatial distribution of hardness and establishing correlations with microstructural and morphological features. Leveraging Gaussian process regression, we quantified the variation in spatial hardness, providing a comprehensive understanding of the material's mechanical behavior. This study establishes a foundation for elevating the wear resistance of DED-printed 316L through the innovative approach of ultra-fast boriding, paving the way for advancements in additive manufacturing applications.

1. Introduction

The critical need for surface coatings in DED applications becomes evident in addressing challenges related to hardness and wear resistance. Coatings play a pivotal role in enhancing the durability of DED-manufactured components, effectively mitigating issues associated with the susceptibility of 316L stainless steel to wear. These coatings, synthesized through diverse methods, offer a combination of desirable properties, including high hardness and wear resistance, thermal stability, diffusion barrier capabilities, and, in certain instances, low friction [1]. Moreover, surface coatings are critical for enhancing the performance of various tools and components in applications ranging from cutting, forming, and casting tools to automotive and aerospace components [2]. The use of coatings can help improve the wear resistance of these components, thereby increasing their lifespan and reducing the need for frequent replacements.

An innovative approach to enhance the hardness and wear resistance of additively manufactured (AM) components is through the use of ultra-fast boriding [3]. Numerous studies have investigated the enhancement of wear resistance in stainless steels through the formation of boride layers containing compounds such as NiB, CrB, NbB, and FeB [4–8]. These layers have demonstrated efficacy in improving material durability, particularly at both room and high temperatures.

Conventional boriding techniques, such as pack, box boriding, as well as Chemical Vapor Deposition (CVD) and Physical Vapor Deposition (PVD) are well-established in the industry. However, the ultra-fast boriding process introduces a significant departure from these traditional methods. This process uses an electrochemical molten-salt technique, eliminating the need for toxic gases and the production of hazardous waste. It also allows for the reuse of the same salt multiple times, marking a significant advancement in environmental sustainability. Executed at elevated temperatures typically between 800 °C and 1000 °C [9], this process dramatically reduces the processing time from several hours to minutes. The introduction of boron into the substrate material at these temperatures leads to a reaction with the base metal, forming a hard, wear-resistant surface layer. This short duration process results in a uniform and dense boride layer with excellent wear resistance and hardness properties, often enhancing the quality of the boron-rich surface without compromising its integrity.

Notably absent from existing literature is an exploration of ultra-fast

☆ 52nd SME North American Manufacturing Research Conference (NAMRC 52, 2024)

* Corresponding author.
E-mail address: satish@tamu.edu (S.T.S. Bukkapatnam).

https://doi.org/10.1016/j.jmapro.2024.04.094
Received 10 April 2024; Accepted 30 April 2024
Available online 18 May 2024

boriding applied to stainless-steel structures produced through the DED. This research gap underscores the novelty of the current study, positioning it as a first effort to elucidate the impact of ultra-fast boriding on DED-produced stainless steel. The application of ultra-fast boriding holds considerable promise in enhancing the hardness and wear resistance of AM-manufactured components, potentially rendering them more reliable and durable in demanding operational environments.

Hardness stands out as a frequently tested mechanical property due to its quick and relatively inexpensive measurement, offering valuable insights into other properties like yield strength and wear resistance [10]. When it comes to AM components, literature often presents scattered data on mechanical properties such as yield strength, primarily stemming from internal defects [11]. In contrast, micro-hardness data remain largely unaffected by these internal defects. Consequently, hardness measurements provide a more accurate reflection of the actual impact of microstructural features, encompassing factors such as the presence of different phases, precipitate particles, average grain size, and alloy composition.

Given the inherent microstructural heterogeneity of DED-printed components, it becomes essential to uncover the spatial variation in hardness within boride-coated DED-printed 316L [12]. Understanding how hardness is distributed across these complex structures is paramount for ensuring consistent material performance and reliability in diverse application scenarios. This study aims to dissect this intricate relationship, shedding light on the spatial microhardness distribution and morphological features that underpin the performance of boride-coated DED-printed 316L components.

The main contribution of this paper is as follows:

1. This study is perhaps the first to investigate ultra-fast boriding on DED-printed 316L. The spatial variation in microhardness is correlated with the microstructure and morphological features.
2. The uncertainty in microhardness was quantified using Gaussian process regression (GPR). This quantification is important as it helps to understand how the standard deviation of hardness varies on a particular surface, which can be correlated with the microstructure heterogeneity and morphological features of the surface.

The remainder of this paper is organized as follows. Section 2 presents detailed experimental methodologies, while Section 3 presents the spatial characteristics such as microhardness and morphological patterns of borided DED-printed 316L; concluding remarks are summarized in Section 4.

2. Experimentation details

2.1. Directed energy deposition

The experimental setup as shown in Fig. 1 involved the fabrication of cubic stainless steel 316L samples with dimensions of 10 mm using an Optomec-LENS® MTS 500. This machine tool operates as a 4-axis CNC system, automating the control of the worktable in the X and Y directions, the motion of the laser and a milling head along the Z (vertical) axis, and the rotation of a horizontal spindle. Notably, it offers versatile capabilities for cladding and repairing worn-out components.

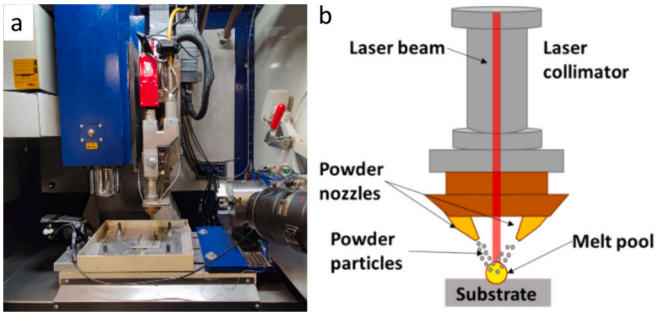

Fig. 1. (a) smart manufacturing platform - Optomec Hybrid MTS 500; (b) schematic representation of DED process, showcasing the fundamental setup and methodology.

The machine is equipped with an IPG YLR-1000 fiber laser with a spot size of 600 μm and a wavelength of 1070 nm. Additionally, it incorporates two powder feeder hoppers, extendable to four, from which powder is conveyed to a mixing chamber. The powder is then delivered through four nozzles employing pressurized argon. This inert gas not only facilitates powder transport and delivery but also plays a crucial role in minimizing oxidation during deposition and serves as a shielding gas throughout the process. Importantly, the machine is designed to maintain oxygen levels in the chamber below 40 ppm.

For the specific experiments conducted, an open atmosphere (OA) mode was employed. In this mode, a highly focused laser beam interacts with the powder particles, creating a melt pool that solidifies in the direction of the scan. Control over the process is facilitated by a Siemens 828D controller, offering adjustment capabilities for various parameters including powder composition, powder feed rate, laser power, hatch spacing, scan speed, and dwell time.

In this study, AISI Stainless Steel 316L powder particles, with diameters ranging from 44 to 106 μm, were used to print cubical parts (10 mm in length). Two distinct sets of process parameters were employed to fabricate these parts, as summarized in Table 1. The selection of these parameters was driven by their potential to yield different microstructures, facilitating an analysis of how the boriding process is affected by variations in the sub-surface microstructure and morphology. For example, Balhara et al. [13] showed distinct differences in microstructure and morphological texture associated with different parameter settings. Notably, the texture was fine columnar dendritic at 300 W and coarse columnar dendritic formations interspersed with cellular structures at 450 W.

The selection of specific boriding parameters (such as temperature, time, current density, and salt composition) is critical to achieving the desired properties in the treated material. In this study, the parameters were chosen based on guidance from previous works [14,15]. Consequently, to isolate the impact of these microstructural differences, the boriding process parameters were maintained constant.

2.2. Boriding procedure

DED-printed 316L samples with the power level of 300 W and 450 W were treated using the Ultra-fast boriding technique. Before boriding mechanical polishing was carried out in multiple steps using a Buehler Automet 250 polisher. Initial polishing steps, conducted at 100 rpm, involved the use of 800, 1000, and 1200-grade emery pads. The final polishing stage, performed at 50 rpm, utilized a microcloth and colloidal silica to achieve a refined finish.

As shown in Fig. 2, the boriding of samples was performed using a molten salt electrolyte consisting of 90 % wt. borax and 10 % wt. sodium carbonate. A 2-electrode system was employed for the electrolysis, with a graphite crucible functioning as the anode and DED-printed 316L samples serving as the cathode. The process was conducted at a current density of 200 mA/cm^2 and a temperature of 1000 °C for 15 min. Following the electrolysis, samples were removed from the crucible, air-cooled, and washed in hot water until the remaining electrolyte dissolved from the specimen surface.

Table 1
Process parameters were used to print 316L samples and later borided using ultra-fast boriding.

Sample	Laser power (W)	Scan speed (mm/s)	Linear energy density (J/mm)
1	300 W	7.40	40.54
2	450 W	4.65	96.77

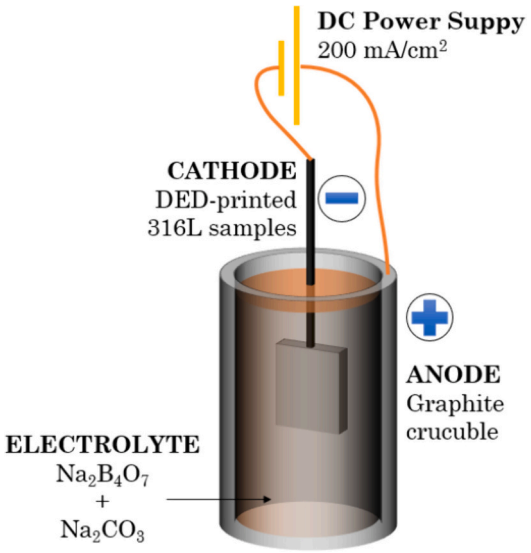

Fig. 2. Schematic view of the electrochemical cell for Ultra-fast boriding technique.

2.3. Characterization procedure

To prepare these chosen samples for subsequent analyses, they were embedded in epoxy resin, ensuring a cross-sectional surface exposure for subsequent polishing. The standard metallurgical sample preparation procedure was followed for both hardness and microstructure studies. The same polishing procedure is discussed in Section 2.2.

Observation of the microstructure in polished and etched cross-sections of the samples was conducted using an Olympus BX-51 optical microscope (OM). To further characterize the samples, microhardness profiles were determined across the polished cross-sections. The Vickers method was employed for microhardness measurements, utilizing a LECO LM110 AT instrument. Testing conditions adhered to ASTM E92 standards, employing a load of 25 gf with a dwell time of 13 s. The phase composition of boride layer was characterized from the surface of the samples by a Rigaku MiniFlex X-ray diffractometer (XRD) using Cu-Kα radiation (40 kV, 15 mA) with a scanning speed of 5°/min.

3. Results

3.1. Microstructure and morphological features of DED-printed 316L

The microstructure of the DED-printed 316L exhibits interesting characteristics, marked by a combination of fine and coarse columnar dendritic structures. This unique arrangement can be attributed to the localized heating and rapid solidification inherent to the DED process. The laser-induced melting followed by rapid cooling creates conditions conducive to the formation of such diverse dendritic structures, presenting a visual manifestation of the complex thermal gradients experienced during printing.

As shown in Fig. 3(a,b), at a power level of 300 W, the microstructure exhibited a low degree of heterogeneity, characterized by a uniform distribution of fine columnar dendritic grains. In contrast, an increase in power to 450 W resulted in a high degree of heterogeneity, evident in the formation of coarse columnar dendritic grains as shown in Fig. 3(c,d). Beyond microstructure, morphological features, specifically ripples observed on the surface of the DED-printed 316L played a significant role.

Ripples, surface waves forming along the scan tracks, displayed a notable connection with the distribution of columnar dendritic grains at the ripple boundary [13]. The observed variations in ripple wavelength between 300 W and 450 W underscored the sensitivity of these features to specific printing parameters. Notably, the ripple wavelength at 300 W measured 0.50 mm, contrasting with the 1.81 mm wavelength at 450 W. This implies that smaller ripple spacing corresponds to minimal

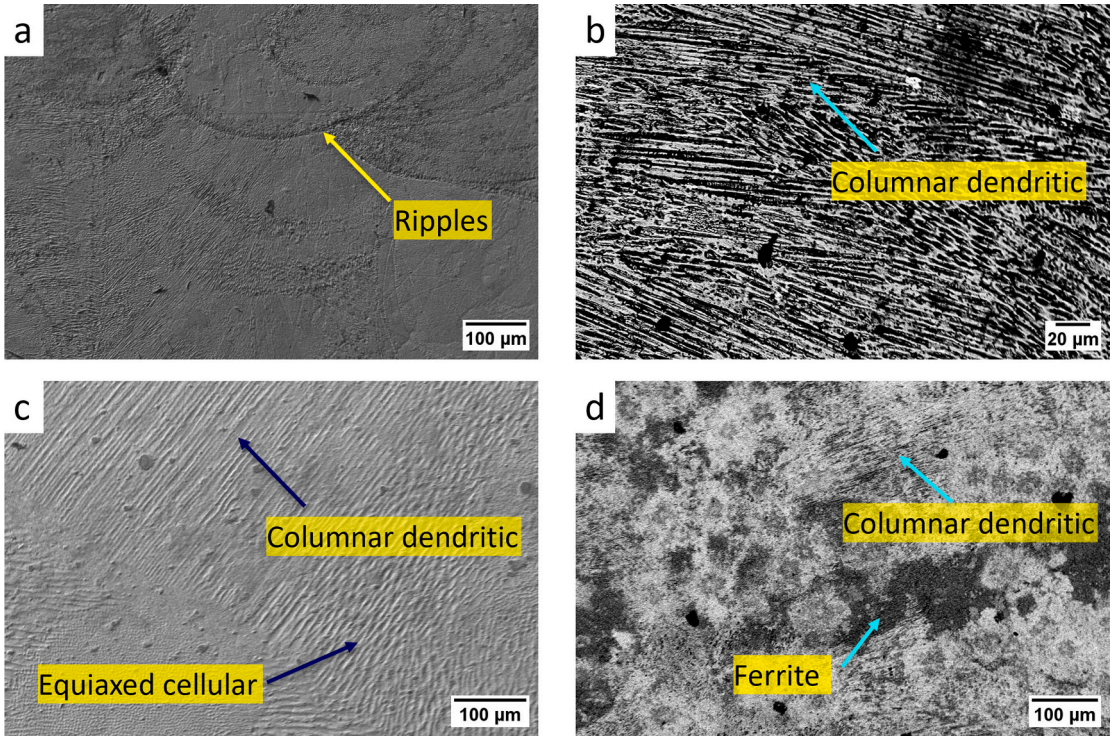

Fig. 3. (a,b) Scanning Electron Microscopy (SEM) and High-Resolution Backscattered Electron Imaging (HBSD) images of sample 1 printed at 300 W, providing detailed insights into surface ripples, phase distribution, and sample composition; (c,d) SEM and HBSD images of Sample 2 printed at 450 W, elucidating microstructural features and highlighting the presence of heavy elements like Chromium (Cr) and Molybdenum (Mo) within the 316L substrate.

variation in heterogeneity. Consequently, at 300 W, the distribution of fine columnar dendritic structures exhibited minimal variation in the hardness of the substrate as discussed in Section 3.3.

3.2. Boride coating effects on microstructure and morphological features

Upon boriding the DED-printed 316L samples, notable alterations in both microstructure and morphology are observed. A distinct boride layer, measuring approximately 20 μm in thickness, is observed to form on the surface of the 316L substrate, as shown in Fig. 4. This layer exhibits a remarkable hardness of 2200 HV ± 200, representing a significant enhancement over the initial surface of the DED-printed 316L material. Micrographs presented in Fig. 4(a,c) illustrate multiple zones within the coating and substrate. The top layer of the boride, appearing darker in coloration, is predominantly comprised of the FeB phase, owing to its higher boron content. Conversely, the subsequent, lighter-colored layer primarily consists of the Fe_2B phase. Notably, the phases identified can be further corroborated through XRD analysis.

The diffusion zone, measured by a thickness of approximately 5 μm, serves as an interface between the boride layer and the 316L substrate, facilitating the transition between the boriding and 316L substrate. Moreover, microscopic analysis reveals the presence of small pores and pits, particularly between the Fe_2B layer and the diffusion zone, with radii ranging from 0.1 to 0.8 μm. These features highlight potential areas of interest for further optimization of the boriding process to mitigate microstructural irregularities and enhance coating integrity. Remarkably, the absence of cracks within this region indicates a robust bond between the boride coating and the substrate.

This stratified composition reflects the complexity of the boriding process and suggests distinct phases of boron diffusion and reaction with the substrate material. Fig. 4(b,d) illustrates the diffusion of boron through the grain boundaries. The diffusion patterns are inherently influenced by the microstructural characteristics of the deposited 316L material, such as grain boundary distribution. A notable difference is evident between sample 1, as depicted in Fig. 4(b), and sample 2, as shown in Fig. 4(d), particularly in terms of grain boundary concentration. Sample 1 shows a higher density of grain boundaries compared to sample 2. Consequently, this higher density leads to more penetration of boron atoms in sample 1 than in sample 2. This difference underlines the direct impact of grain boundary density on the diffusion behavior of boron atoms within the substrates.

XRD analysis presented in Fig. 5 confirms that the coating layer consists of FeB, Fe_2B, and Ni_3B phases. In the XRD pattern of Sample 2, the (120) plane's peak aligns precisely with the reference, indicating a uniform crystal structure and phase formation (Fig. 5). However, in Sample 1, the (120) peak shows a slight deviation, which suggests not only an irregular formation of the FeB phase but also potential stress within that layer. Such stress or structural inconsistency in the FeB phase

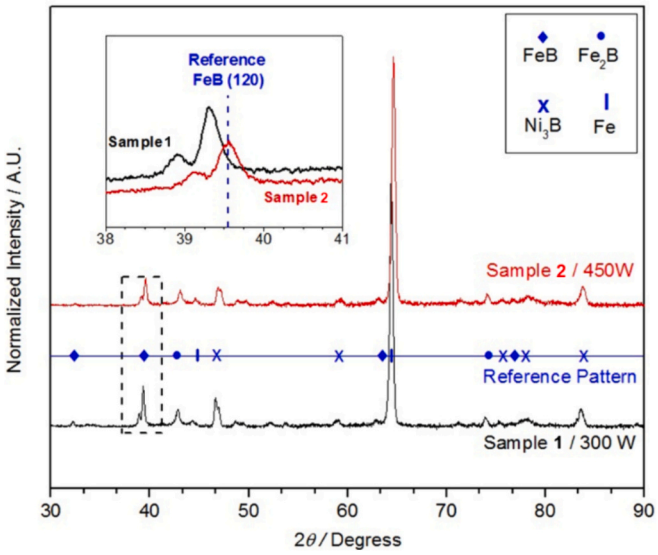

Fig. 5. XRD patterns obtained from the borided DED-printed 316L.

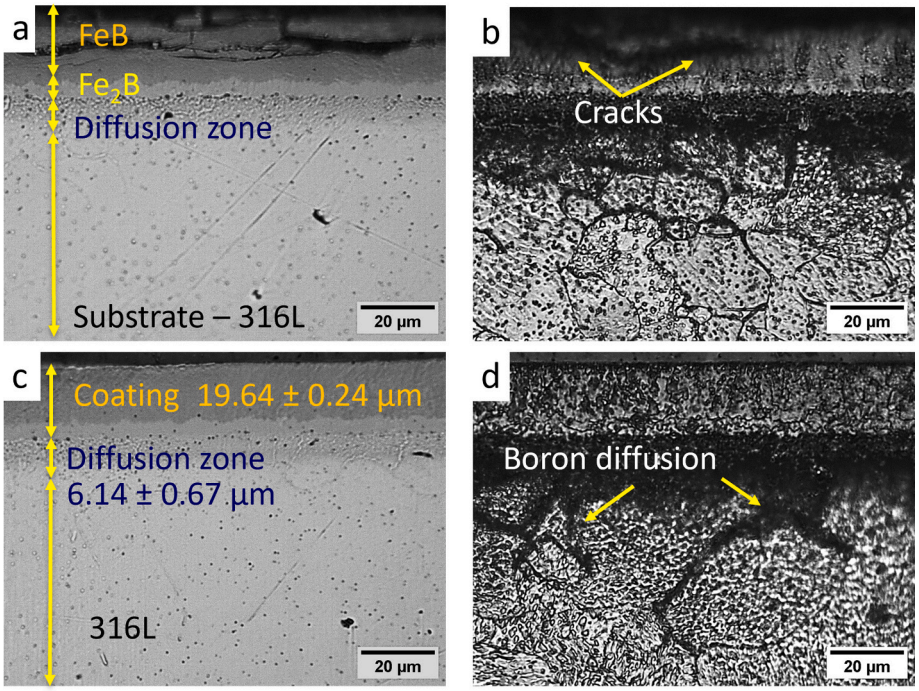

Fig. 4. Optical micrographs depicting the surface morphology of the coating and diffusion zone, illustrating the diffusion of boron atoms through grain boundaries. In (a, b), the presence of cracks is evident in the coating of Sample 1, highlighting potential stress accumulation in the FeB layer. Micrographs in (b, d) illustrate the boron diffusion along the grain boundaries.

could lead to the coating's increased susceptibility to cracking under mechanical loads like indentation.

In the subsequent Section, we discuss the spatial microhardness distribution across the boride-coated DED-printed 316L samples, aiming to elucidate the correlation between microstructural variations and mechanical properties.

3.3. Spatial microhardness distribution

The investigation of spatial variation in hardness assumes significance in comprehending the performance of components subjected to diverse load conditions. To elucidate this, Vickers hardness measurements were conducted.

In the sample produced under a laser power of 300 W, distinct variations in the behavior of the FeB layer within the coating were observed across different locations. Fig. 6(a,b) illustrates the presence of radial cracks surrounding the indents, suggesting a propensity for cracking [16]. Intriguingly, in proximity to the Fe_2B sub-layer, no cracks were observed. This observation points to a potential divergence in mechanical behavior between the FeB and Fe_2B phases within the coating, underscoring the complexity of the material's response to localized hardness testing.

As shown in Fig. 6 (c,d), the sample fabricated under a laser power of 450 W exhibited an absence of cracking within the coating, indicating good structural integrity. Subsequently, a comprehensive surface hardness mapping was conducted as shown in Fig. 7.The findings revealed distinct characteristics: Sample 1, produced at 300 W with a microstructure characterized by fine columnar dendritic features, demonstrated a uniformly distributed hardness across the substrate, as depicted in Fig. 7 (a). Contrastingly, significant variations in coating hardness were observed, suggesting the potential formation of different phases within the coating.

Notably, the presence of coarse columnar dendritic structures on the surface of the 316L printed with 450 W resulted in spatial variations in hardness as shown in Fig. 7 (b). However, the coating itself displayed a

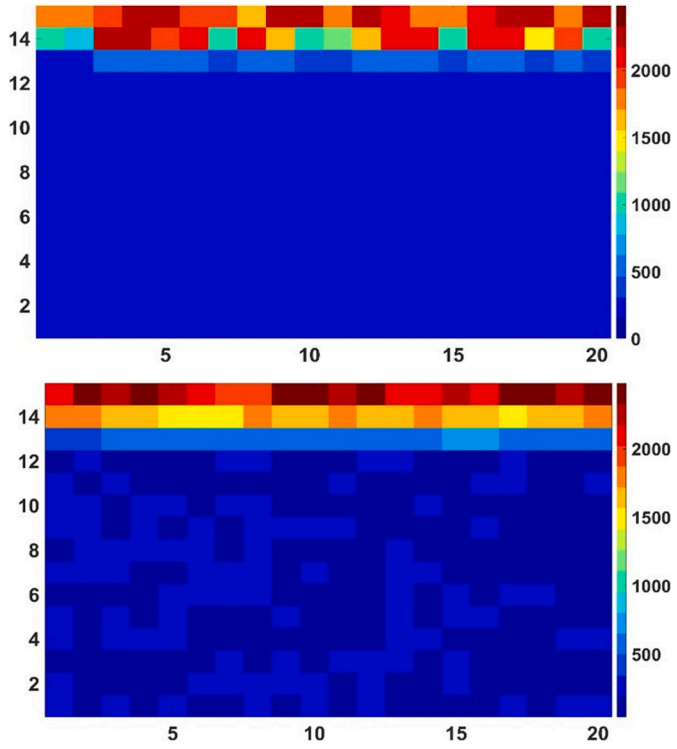

Fig. 7. (a) Spatial variation in hardness observed in Sample 1, showcasing uniform hardness in 316L attributed to the presence of fine columnar dendritic structures, with a notable large variation in hardness within the coating; (b) Uniform hardness observed in the coating of Sample 2 compared to the 316L surface, emphasizing the influence of coarse columnar dendritic structures on spatial hardness distribution.

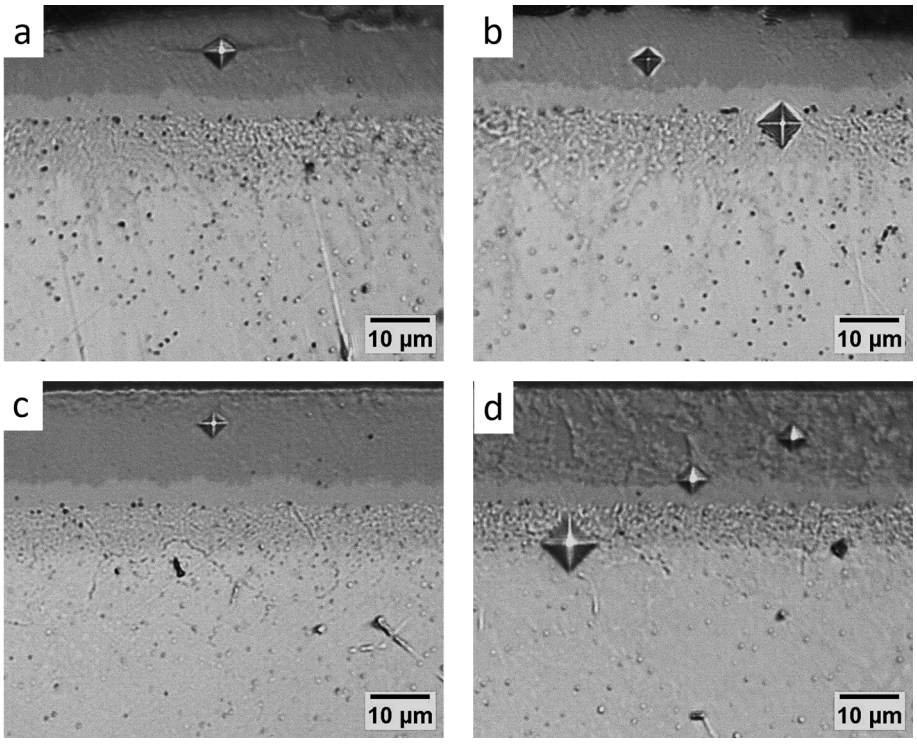

Fig. 6. (a, b) Crack induced by indentation on the coating of Sample 1, indicating localized cracking and implying spatial variation in the hardness of the coating; (c, d) No signs of cracking observed on Sample 2, showcasing a uniform coating on Sample 2.

more consistent hardness profile. Furthermore, the repetitive nature of the microstructure texture, dictated by the surface ripples, directly impacts the spatial hardness of the coating. This discrepancy in hardness characteristics emphasizes the relation between heterogenous microstructure, morphology, and hardness in the DED-printed components.

3.4. Uncertainty quantification using Gaussian Process Regression

To quantify the spatial variation in hardness across the samples, Gaussian Process Regression (GPR) was employed. GPR serves as a robust statistical tool capable of modeling complex relationships between variables. In this study, the application of GPR was important for capturing and analyzing the nuanced patterns in hardness data. By utilizing spatial coordinates and corresponding hardness values, GPR facilitated the formation of a probabilistic model that not only discerned the mean trend in hardness but also provided valuable insights into the uncertainty associated with each prediction.

The spatial representations generated through GPR not only visualize the observed changes in hardness but also offer a statistical foundation for interpreting the influence of microstructural features and printing parameters on the mechanical properties of the samples. Specifically, an ardexponential kernel function was employed in the GPR analysis.

Fig. 8 presents the GPR plots illustrating the variations in hardness across both substrates in the x-direction (along sample length), exhibiting a correlation with the ripple spacing and amplitude. Notably, Sample 2 showcased a ripple spacing of 1.81 mm, whereas Sample 1 demonstrated a spacing of 0.5 mm, as derived from our previous study. The GPR analysis of hardness reveals localized increases in hardness, attributed to the presence of ripple boundaries comprised of columnar dendritic grains. Examination of the GPR mean and uncertainty quantification bands indicate a spacing or wavelength of 1.33 mm, showing a notable resemblance to the ripple wavelength.

Furthermore, Fig. 9 presents results from 3D Gaussian process regression, where a significant increase in coating hardness as compared

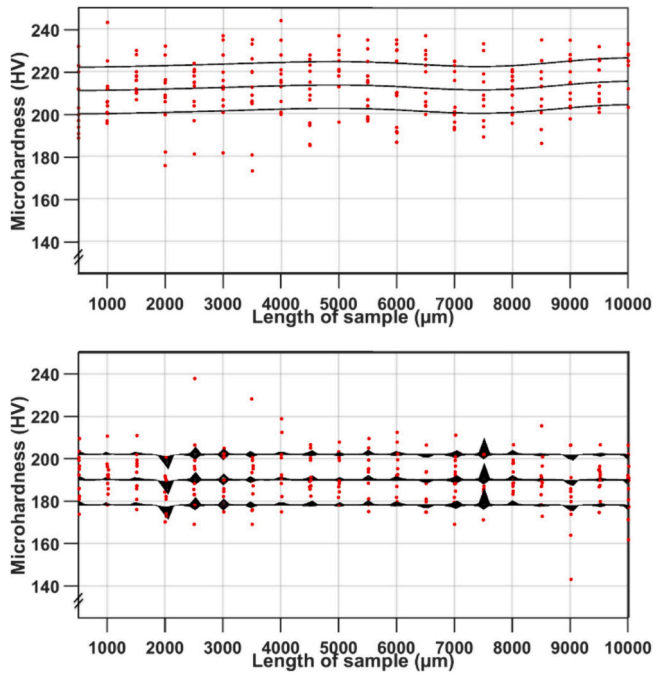

Fig. 8. Gaussian process regression illustrating hardness variations in substrates: (a) Sample 1, exhibiting a fine columnar dendritic structure, demonstrating a higher mean hardness of 212 HV (σ = 13); (b) Sample 2, characterized by coarse columnar dendritic structure, displaying a mean hardness of 189 HV (σ = 15).

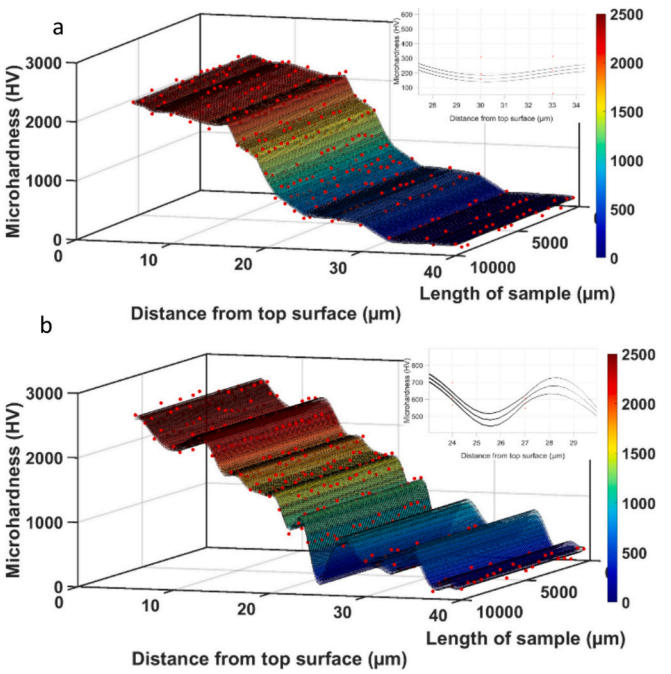

Fig. 9. Gaussian Process Regression was employed to quantify the spatial variation in hardness. (a) Smooth variation (SD 56) was observed for Sample 1; (b) A pronounced variation (SD 126) as a function of the y-direction was noted for Sample 2, attributed to the larger spacing of ripples introducing increased heterogeneity on the surface.

to substrate can be observed. The results, as depicted in Fig. 9 (a), reveal a smoothly varying hardness distribution in the sample produced under 300 W. Notably, the hardness is identified as a function of the y-direction (build direction + coating), with slight variations observed in the x-direction as noted in Fig. 8. This y-directional variation is strongly correlated with the distribution of grains on the surface, reflecting the influence of microstructural features.

Conversely, in Sample 2, printed at 450 W, a more pronounced variation with a standard deviation of 126 in hardness along the y-direction was observed, as shown in Fig. 9 (b). This variation can be attributed to the presence of a spread of coarse columnar dendritic structures on the surface. Additionally, the greater ripple spacing in this sample contributes to increased heterogeneity in the microstructure, further influencing the observed variations in hardness.

4. Concluding remarks

This experimental study is perhaps the first to examine boride coating applied to DED-printed 316L components. It addresses a critical knowledge gap by extending the understanding of how boride coating, known for enhancing material hardness, interacts with the unique microstructures produced through DED printing. By characterizing the key morphological and microstructural attributes of the boride coating on DED-printed 316L components, this research provides detailed insights into how these attributes influence the spatial distribution of hardness, accompanied by suitable uncertainty quantification.

The laser-material interaction gives rise to a complex thermo-mechanical phenomenon, which, in turn, is responsible for shaping the observed microstructure and morphological features. The presence of these distinct surface features contributed to significant fluctuations in spatial variation in hardness. These variations underscore the importance of printing parameters in determining the microstructure and surface morphology of DED-printed 316L components.

The presence of cracks in the FeB layer at 300 W can be attributed to the higher concentration of grain boundaries facilitating enhanced

boron diffusion. During the diffusion process, it introduces stresses within the material, particularly at the interfaces between different phases and along the grain boundaries. These stresses can manifest as cracks, especially in regions where the coating experiences mechanical and thermal loading. Importantly, XRD analysis confirms the presence of stress accumulation in the FeB layer of sample 1.

Surface irregularities, such as the wavy pattern texture resulting from ripples, disrupt the uniform diffusion of boron atoms, leading to coatings with inconsistent properties. The study finds a correlation between the frequency of ripples and the variation in spatial hardness across the coating. Specifically, sample 1 exhibits high-frequency ripples associated with larger variations in hardness, whereas sample 2, with longer ripple wavelengths, shows minimal hardness variation. This observation highlights how heterogeneity in surface texture and microstructure affects boron diffusion kinetics and microstructural evolution.

The observed variation in spatial hardness in the coating of sample 1, printed at a linear energy density of 40 J/mm, notably at 300 W, is primarily due to the presence of high-frequency ripples on the surface. These ripples disrupt the uniformity of the surface, creating an uneven topography, which leads to variations in the hardness of the coating across different areas. Surfaces characterized by these high-frequency patterns are not as smooth, affecting the evenness of the coating application and, consequently, the uniformity of its hardness.

In contrast, sample 2, with lower frequency ripples, indicative of a smoother surface, allows for a more homogeneous application of the coating, leading to a more consistent hardness distribution. Adjusting the process parameters to control the presence and frequency of ripples can significantly impact the quality and performance of coatings on DED-printed components.

The main takeaways from this study are summarized as follows:

1. The boriding process led to the formation of a distinct boride layer, approximately 20 μm thick, on the 316L surface. Microhardness testing studies suggested that these layers exhibited an impressive hardness of 2200 HV, marking a tenfold increase compared to the hardness of the 316L surface. Notably, this hardness value is 31.18 % higher than that achieved through the boriding of wrought 316L using an electrochemical process.
2. The boride layer comprised of multiple contrasting sub-layers. The top layer, rich in FeB phase, appeared darker in color, while the subsequent layer, predominantly consisting of Fe_2B phase, showed a lighter coloration. A diffusion zone, approximately 5 μm in thickness, serves as the transition between the boride layer and the 316L substrate.
3. Microscopic analysis of the diffusion zone between the boride layer and the 316L substrate revealed no cracks, indicating good adhesion and structural integrity. Notably, small pores and pits with diameters ranging from 0.1 to 0.8 μm were detected specifically between the Fe_2B layer and the diffusion zone. These observed imperfections could suggest localized variations in boron diffusion or reactions within these interface areas.
4. The contrasting settings of laser power and linear energy during DED printing of the two samples considered in this study have resulted in distinct microstructures for the samples. The sample printed at 300 W laser power with 40 J/mm linear energy, displayed a fine columnar dendritic structure. The sample printed at 450 W laser power with 95 J/mm linear energy, exhibited a coarse columnar dendritic structure. These differences in printing conditions resulted in notably different coating morphologies and hardness distributions across the samples.
5. Microhardness analysis using Vickers hardness testing revealed spatial variability in hardness among the samples. Gaussian process regression analysis showed a more consistent hardness distribution in sample 1 (SD of 13) across the substrate as compared to Sample 2 (SD: 15). Additionally, sample 1 exhibited a significantly higher mean hardness of 212 HV compared to sample 2, which recorded a mean hardness of 189 HV.

It is essential to underscore that this investigation contributes significantly not only to the fundamental understanding of the relationship between microstructure, morphology, and hardness in DED-printed materials but also carries practical importance. For example, the boriding process enhances 316L stainless steel with superior properties, including a surface hardness of 2000–2200 Hv, excellent hardness retention at high temperatures, low friction coefficient, and robust corrosion resistance which is suitable for biocompatibility in implants [7]. Moreover, the higher hardness of boride coatings makes them suitable choices for increasing the durability of cutting tools [17], expanding their applications in various industrial sectors. By venturing into the unexplored territory of applying boride coatings to DED-printed samples, this study lays the groundwork for potential advancements in material optimization for additive manufacturing applications.

CRediT authorship contribution statement

Himanshu Balhara: Data curation, Formal analysis, Investigation, Visualization, Writing – original draft. **Cagatay Yelkarasi:** Data curation, Investigation, Writing – original draft. **Ali Erdemir:** Supervision, Validation, Writing – review & editing. **Satish T.S. Bukkapatnam:** Conceptualization, Funding acquisition, Supervision, Validation.

Declaration of competing interest

The authors declare that they have no known competing financial interests or personal relationships that could have appeared to influence the work reported in this paper.

Acknowledgments

The authors would like to acknowledge the support from National Science Foundation (FMRG grant award #2328395) and Rockwell International Professorship. This material is partially based on work supported while serving at the National Science Foundation. Any opinions, findings, conclusions, or recommendations expressed in this material are those of the author(s) and do not necessarily reflect the views of the National Science Foundation.

References

[1] Kulka M, Mikolajczak D, Makuch N, Dziarski P, Miklaszewski A. Wear resistance improvement of austenitic 316L steel by laser alloying with boron. Surf Coat Technol Apr. 2016;291:292–313. https://doi.org/10.1016/j.surfcoat.2016.02.058.
[2] Farfan-Cabrera LI, Reséndiz-Calderón CD, Hernandez-Peña A, Campos-Silva I, Gallardo-Hernández EA, Contla-Pacheco AD. Tribological effects of boriding treatment on a low carbon steel repaired by wire and arc additive manufacturing. Surf Coat Technol Jul. 2023;465:129574. https://doi.org/10.1016/j.surfcoat.2023.129574.
[3] S. Timur, G. Kartal, O. L. Eryilmaz, and A. Erdemir, "Ultra-fast boriding of metal surfaces for improved properties," Argonne National Laboratory (ANL), Argonne, IL (United States), 8,951,402, Feb. 2015. Accessed: Nov. 15, 2023. [Online]. Available: https://www.osti.gov/biblio/1350957.
[4] Günen A, Gürol U, Koçak M, Çam G. A new approach to improve some properties of wire arc additively manufactured stainless steel components: simultaneous homogenization and boriding. Surf Coat Technol May 2023;460:129395. https://doi.org/10.1016/j.surfcoat.2023.129395.
[5] Nishimoto A, Kubo T. Boronizing of AISI 316L stainless steel using spark plasma sintering technique. DDF Nov. 2020;405:3–10. https://doi.org/10.4028/www.scientific.net/DDF.405.3.
[6] Campos-Silva I, Bernabé-Molina S, Bravo-Bárcenas D, Martínez-Trinidad J, Rodríguez-Castro G, Meneses-Amador A. Improving the adhesion resistance of the boride coatings to AISI 316L steel substrate by diffusion annealing. J Mater Eng Perform Sep. 2016;25(9):3852–62. https://doi.org/10.1007/s11665-016-2201-6.
[7] Özbek I, Konduk BA, Bindal C, Ucisik AH. Characterization of borided AISI 316L stainless steel implant. Vacuum May 2002;65(3):521–5. https://doi.org/10.1016/S0042-207X(01)00466-3.

[8] Goeuriot P, Thevenot F, Driver JH. Surface treatment of steels: Borudif, a new boriding process. Thin Solid Films Mar. 1981;78(1):67–76. https://doi.org/10.1016/0040-6090(81)90418-1.
[9] Kahvecioglu O, Sista V, Eryilmaz OL, Erdemir A, Timur S. Ultra-fast boriding of nickel aluminide. Thin Solid Films Dec. 2011;520(5):1575–81. https://doi.org/10.1016/j.tsf.2011.08.077.
[10] Zuback JS, DebRoy T. The hardness of additively manufactured alloys. Materials Nov. 2018;11(11):11. https://doi.org/10.3390/ma11112070.
[11] Petrescu MI. Nanohardness and microhardness: some specific mechanical effects. UPB Sci Bull B Chem Mater Sci Jan. 2003;65:43–54.
[12] Kayali Y, Büyüksağiş A, Yalçin Y. Corrosion and wear behaviors of boronized AISI 316L stainless steel. Met Mater Int Sep. 2013;19(5):1053–61. https://doi.org/10.1007/s12540-013-5019-x.
[13] Balhara H, Botcha B, Wolff SJ, Bukkapatnam STS. Ripple formations determine the heterogeneous microstructure of directed energy deposition (DED)-printed 316L components. Mater Des Mar. 2023;227:111756. https://doi.org/10.1016/j.matdes.2023.111756.
[14] Kartal G, Timur S, Eryilmaz OL, Erdemir A. Influence of process duration on structure and chemistry of borided low carbon steel. Surf Coat Technol Nov. 2010;205(5):1578–83. https://doi.org/10.1016/j.surfcoat.2010.08.050.
[15] Kartal G, Eryilmaz OL, Krumdick G, Erdemir A, Timur S. Kinetics of electrochemical boriding of low carbon steel. Appl Surf Sci May 2011;257(15):6928–34. https://doi.org/10.1016/j.apsusc.2011.03.034.
[16] Li H, Bradt RC. The effect of indentation-induced cracking on the apparent microhardness. J Mater Sci Feb. 1996;31(4):1065–70. https://doi.org/10.1007/BF00352908.
[17] Rodríguez-Castro G, Campos-Silva I, Chávez-Gutiérrez E, Martínez-Trinidad J, Hernández-Sánchez E, Torres-Hernández A. Mechanical properties of FeB and Fe2B layers estimated by Berkovich nanoindentation on tool borided steel. Surf Coat Technol Jan. 2013;215:291–9. https://doi.org/10.1016/j.surfcoat.2012.05.145.